Inferno Worlds

Ridden - Harper, A.

1 Introduction

1.1 Summary

A remarkable population of short period transiting rocky exoplanets with equilibrium temperatures on the order of 2,000 K has recently been discovered. They have masses ranging from approximately 8 $M_\oplus$, such as the hot super-Earth 55 Cancri e, to possibly that of Mercury or smaller, such as Kepler-1520 b. Their high temperatures make them very different to the planets in our Solar System. In particular, hot super-Earths are thought to have mineral atmospheres that are produced by the vaporisation of their surfaces, or large exospheres that are produced by sputtering of their exposed surfaces by intense stellar winds. Additionally, some smaller, low surface gravity hot rocky exoplanets have been found to be actively disintegrating and forming 'comet-like' dust tails that produce asymmetric transit light curves with forward scattering features.

These enigmatic objects inspire many questions such as: How did they form? How will they evolve? What is their composition and internal structure? What processes control their mass-loss?

Such fundamental questions can potentially be addressed to a far greater extent for hot rocky exoplanets than is currently possible for cooler rocky exoplanets because their atmospheres and released gas and dust can be observed, presenting the tantalising prospect of directly probing the composition of rocky planets.

The purpose of this thesis is to work towards answering these questions by searching for gas around hot rocky exoplanets with observational spectroscopy (Chapters 2 and 5), and by modelling the transit light curves produced by their 'comet-like' dust tails (Chapters 3 and 4).

1.2 Overview of the field

The first extra solar planetary system was discovered in 1992 (Wolszczan & Frail 1992) and consisted of a 2.8 $M_\oplus$ and a 3.4 $M_\oplus$ planet orbiting a millisecond radio pulsar. These planets could be identified because their orbits induce a variation in

the time-of-arrival of the pulsar's pulses. Pulsar timings can be accurately measured, which enabled the signal of the planets to be detected. However, it is an exotic and unusual system, as pulsars have previously gone through a supernova explosion. The planets possibly formed from the remnants of the supernova explosion (e.g. Lin et al. 1991).

The era of mainstream exoplanet discovery started in earnest in 1995 with the discovery of a $\gtrsim$0.5 Jupiter-mass planet orbiting the main-sequence star 51 Pegasi with an orbital period of 4.2 days, placing it well within the orbit of Mercury in our own Solar System. The existence of a Jupiter mass gas giant planet at such a short orbital distance came as a surprise because our Solar System only has gas giants at significantly larger distances. It is still not completely understood how these 'hot-Jupiters' form, however, the favoured models involve planetary migration (Dawson & Johnson 2018).

51 Pegasi b was discovered with the radial velocity method, which uses the fact that gravitationally bound objects orbit their common centre of mass. In a situation like a planetary system, where the host star is many orders of magnitude more massive than the planets, the centre of mass (or barycentre) is inside the star (but not at its centre). This means that the host star will exhibit small periodic changes in velocity, which can be described with a sinusoid of semi-amplitude, K, given by

$$K = \left(\frac{2\pi G}{P_{orb}}\right)^{\frac{1}{3}} \frac{M_p \sin(i)}{(M_s + M_p)^{\frac{2}{3}}} \frac{1}{\sqrt{1-e^2}} \tag{1.1}$$

where G is the universal gravitational constant, P_{orb} is the planet's orbital period, M_p is the mass of the planet, M_s is the mass of the host star, e is the planet's orbital eccentricity and i is the planet's orbital inclination (e.g. Wright 2017).

This equation shows that K is largest if the planet has a short orbital period and large mass, explaining its sensitivity to 51 Pegasi b. The inclination, i, is the angle between the normal of the planet's orbital plane and the line of sight. Therefore, it is most sensitive to planets in near edge on orbits. Radial velocity measurements allow the planet's mass to be determined if it is a transiting planet, since $\sin(i) \approx 1$.

In the years since the first detection of 51 Pegasi b, new technology and methods have enabled the discovery of smaller planets on longer period orbits. At the time of writing, there are 3735 confirmed exoplanets, of which 2327 where discovered by NASA's Kepler Space Telescope[1], which monitored a field of about 150,000 stars to detect the periodic dimming caused by an orbiting planet transiting its host star (Borucki et al. 2010; Koch et al. 2010).

The transit depth is directly proportional to the fraction of the host star's surface that is occulted by the planet. Assuming spherical stars and planets, this can

[1] Retrieved from the NASA Exoplanet Archive.

be written as

$$\frac{\delta F}{F} = \frac{R_p^2}{R_s^2} \tag{1.2}$$

where F is the star's flux when the planet is not transiting, δF is the change in flux caused by the transit of the planet, R_p is the radius of the planet and R_s is the radius of the star. This makes it most sensitive to planets around small stars. For this reason, Earth sized planets in their host star's habitable zone have been detected around small M-dwarf stars (Gillon et al. 2017), but not yet around Sun-like stars.

The transit method also favours planets that have small orbital distances because it is more likely that they will transit their host star due to the geometry of the system. This can be written as the approximate relation

$$P_{tr} \approx \frac{R_s}{a} \tag{1.3}$$

where P_{tr} is the probability of the planet of orbital semi-major axis, a, transiting its host star of radius, R_s. Planets that have small orbital semi-major axes also have short orbital periods, allowing more transits to be observed. Transit depths are typically $\frac{\delta F}{F} \lesssim 1\%$ so repeated transits measurements are often necessary to overcome the noise and make robust detections. Also, more than one transit observation is needed to robustly determine the planet's orbital period.

After about four years of operation, the failure of two of Kepler's reaction wheels meant that it could no longer point accurately enough to continue its original mission. An alternative mission, called K2, was devised that uses Solar radiation pressure on the solar panels to assist with the stabilisation along the unguided axis. This involved reorienting the spacecraft so that it now observes fields along the ecliptic, spending approximately 75 days on each field (Howell et al. 2014). As a consequence, planets discovered by K2 are accessible to ground-based telescopes in both the Northern and Southern hemispheres. This enabled Chapter 5 of this thesis, which describes the use of the European Southern Observatory's Very Large Telescope (VLT) in Chile to observe K2-22 b.

1.3 Planet formation

Fig. 1.1 shows all the known exoplanets in planet-mass and orbital-period space, colour coded according to the method used for their discovery. The population has a large diversity in mass and orbital period that spans several orders of magnitude. The hot rocky exoplanets that are the focus of this thesis are in the lower-left corner of this diagram with orbital periods of less than a day and masses less than 0.025 Jupiter masses (8 Earth masses).

Planet formation theory has made much progress towards understanding the formation processes that lead to this diversity, however it is not yet completely understood. In the case of hot rocky exoplanets, key questions that are not yet answered include: Did they form at their current orbital distance (in-situ) or did they migrate there? If they did migrate, what triggered this migration? Could their formation process be related to that of hot-Jupiters? Are they the cores of hot-Jupiters that have lost most of their atmospheres? Or are they 'failed hot-Jupiters' that were not able to accrete a large amount of gas?

In general, planets are thought to be formed via two possible mechanisms:

1. The core accretion mechanism: dust and planetesimals in the proto-planetary disk coagulate until they reach a mass large enough to initiate a runaway accretion of gas onto the core that proceeds until the gas is dispersed by stellar winds when the star initiates nuclear fusion. (Pollack et al. 1996)

2. The disk instability mechanism: Instabilities in the disk produce over-dense regions that gravitationally attract the surrounding material, building up a planet (Boss 1997).

However, it is not likely that these mechanisms can operate at the orbital distances of short period planets, so migration is needed (e.g Schlichting 2014; Jackson et al. 2018; Dawson & Johnson 2018; Schlichting 2018). However, for hot super-Earths, the extent of this migration is not well understood and could be from <1 au to several au (Schlichting 2018).

The mechanisms proposed to cause migration are torques from gravitational interactions with the disk (e.g. Lin et al. 1996; Jackson et al. 2018) or gravitational interactions between planets (e.g. Chatterjee et al. 2008; Jackson et al. 2018). Interactions with the disk broadly fall into two categories: Type I migration is relevant for Earth-mass planets, such as those considered in this thesis, and results in migration rates that are proportional to the planet's mass and the disk's surface density. Type II migration is relevant for Jupiter-mass planets that have sufficient mass to clear an annular gap in the disk causing the planet's motion to become linked to the viscous evolution of the gas (Ward 1997; Chambers 2009). Migrations from gravitational interactions between planets (planet-planet scattering) are most effective after the disk has dispersed because the disk can damp the gravitational excitations. Once free of the damping effect of the disk, tightly packed systems can rapidly induce high eccentricities in their orbits. Tidal interactions with the host star then act to circularise and shrink their orbits (e.g. Chatterjee et al. 2008; Jackson et al. 2018).

The atmospheres of hot super-Earths have likely evolved and undergone processing throughout their lifetimes. Even if a super-Earth currently has no atmosphere, it is expected to have gained and then lost a gaseous envelope tens of per-

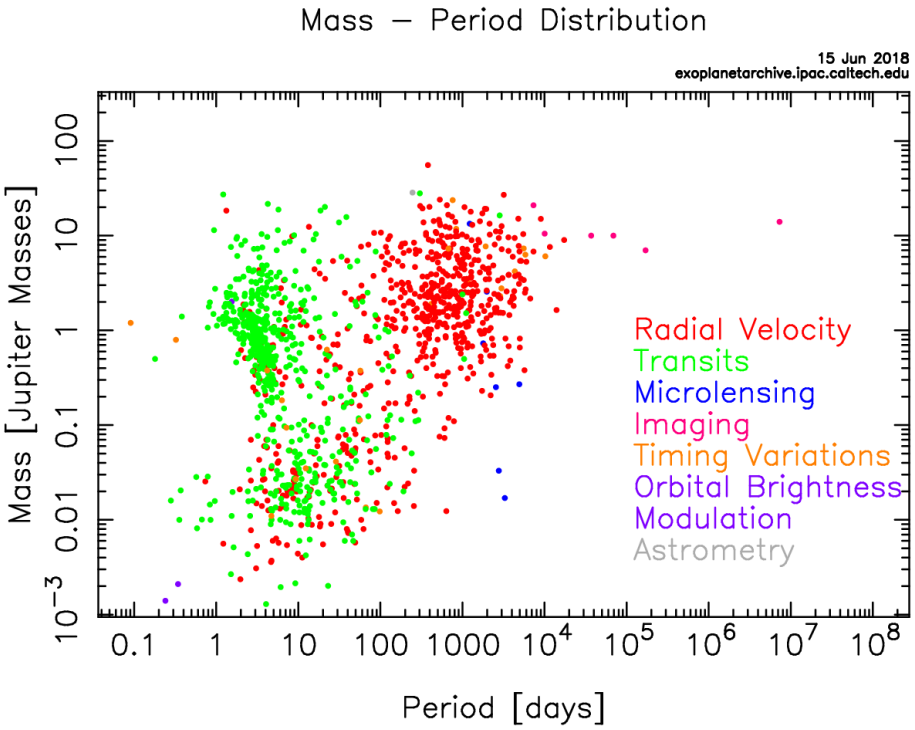

Figure 1.1: The distribution of all known exoplanets in planet-mass and orbital-period space, colour coded according to the method that was used for their discovery. Image credit: NASA Exoplanet Archive.

cent of its core mass, during its formation process (Schlichting 2018). This relates them to the formation of hot-Jupiters, suggesting that they would have become hot-Jupiters if they could have accreted more mass.

1.4 Hot rocky exoplanets

Ultra-short period (< 1 day) rocky exoplanets experience high stellar radiation and potential tidal heating, leading to equilibrium temperatures typically in excess of 2,000 K. Those with masses between a few and $\sim$15 $M_\oplus$ are often called 'hot super-Earths'.

Their high temperatures are sufficient to melt surface rocks, potentially leading to atmospheres composed of their vaporised surfaces (e.g Schaefer & Fegley 2009). Alternatively, if they do not have significant atmospheres, exospheres may be produced by sputtering of their surfaces by stellar winds (Mura et al. 2011). If the gas in these atmospheres or exospheres were to be observed, it would con-

strain the composition of the planet's outer layer, providing valuable information for understanding their formation and evolution. In Chapter 2 of this thesis, we search for sodium and ionized calcium from the atmosphere or exosphere of the hot super-Earth 55 Cancri e.

1.4.1 Sputtering

The Solar System planet Mercury is the closest planet to the Sun, with an orbital semi-major axis of 0.387 au. The orbital distances of short period hot rocky exoplanets are $\gtrsim 25$ times smaller than that of Mercury, so it is intriguing to think of them as being extreme Mercury analogues.

Mercury does not have an atmosphere, but it does have a variable exosphere that is primarily produced by sputtering of its surface. Sputtering is the process of high energy photons or charged particles from the Sun impacting the surface and causing atoms to be ejected. The exosphere of Mercury has been well studied with spacecraft and various telescopes (e.g. Killen et al. 2007), which have robustly detected atoms and ions of elements such as sodium, calcium, potassium and magnesium. The Solar wind and radiation pressure can cause the exosphere to form into a tail, tens of planetary radii long.

Mura et al. (2011) investigated the sputtering induced exospheres of hot rocky exoplanets by simulating the exosphere of CoRoT-7 b and predicted it to be larger than Mercury's and potentially detectable. Motivated by this, Guenther et al. (2011) searched for Na, Ca and Ca^+ in the hot super-Earth CoRoT-7 b but were only able to derive upper limits.

1.4.2 Possible mineral vapour atmospheres

As a result of their high temperatures, hot rocky exoplanets may also have atmospheres that are produced by the vaporisation of their molten surfaces. Schaefer & Fegley (2009) modelled the atmosphere of CoRoT-7 b, which has a mass of 8 $M_\oplus$ and an equilibrium temperature between 1800 and 2600 K, and found that it is likely composed primarily of Na, O_2, O, and SiO gas with lesser amounts of Na and K. They suggest that interactions with the stellar wind may cause large Na and K clouds to surround the planet (similar to those around Mercury and Io), which may potentially be detected with current observing capabilities. Miguel et al. (2011) carried out a similar but more extensive study, considering larger ranges of temperature ($1000 - 3500$ K), planetary mass ($1 - 10$ $M_\oplus$) and planet radius ($1 - 2.5$ $R_\oplus$). They found that the relative abundances of atmospheric species depend significantly on initial composition and temperature. Ito et al. (2015) performed a similar study and calculated atmospheric opacities over the wavelength region of $0.1 - 100$ μm. Their results suggest that a thermal inversion may occur due to UV

absorption by SiO. They estimate that strong SiO features may be detectable with the Spitzer Space Telescope and that Na and K may also be detectable with large ground based telescopes.

Based on the mean density of the hot super-Earth 55 Cancri e, it was thought to possibly have a hydrogen-helium or water atmosphere (e.g. Gillon et al. 2012). Recent non-detections of hydrogen (Ehrenreich et al. 2012), water (Esteves et al. 2017), and a potential detection of Ca^+ (Chapter 2) disfavour these ideas. However, hints of a HCN atmosphere have also been reported, that actually may support the hydrogen-rich interpretation (Tsiaras et al. 2016).

55 Cancri e is a promising target for detailed atmospheric characterisation with stable, high resolution spectrographs because its host star (V = 5.95) is 200 times brighter than CoRoT-7, which only yielded non-detections (Guenther et al. 2011). 55 Cancri e is therefore the subject of Chapter 2 of this thesis.

1.5 Characterisation with spectroscopy

Spectroscopy can constrain the composition of exoplanet atmospheres and exospheres because atoms and molecules absorb and emit light at unique wavelengths that correspond to transitions between quantised energy levels. Spectrographs disperse light and enable the observed flux as a function of wavelength to be measured. The resolving power, R, of a spectrograph determines the smallest difference in wavelength that it can distinguish, $\Delta\lambda$, for a given wavelength λ and is given by

$$R = \frac{\lambda}{\Delta\lambda}. \tag{1.4}$$

The strength of spectral features in an atmosphere generally depend on its scale height, H, which is the vertical distance over which its pressure decreases by a factor of $1/e$, and is given by

$$H = \frac{kT}{\mu_{atm} g'} \tag{1.5}$$

where k is the Boltzmann constant, T is the temperature of the atmosphere, μ_{atm} is the mean molecular weight of the atmosphere and g' is the acceleration due to the planet's gravity (Kaltenegger 2011). This shows that larger scale heights occur for larger temperatures and smaller atmospheric mean molecular weights and gravities.

During transit, star light passes through an annulus of atmosphere around the planet, where it can be absorbed by atmospheric atomic or molecular species.

The level of absorption from such features can be estimated as

$$\delta F_{tr} = \frac{(R_p + nH)^2 - R_p^2}{R_s^2} \tag{1.6}$$

where n is the thickness of the atmospheric annulus in scale heights and is typically $5 - 10$. Substituting in typical values gives $\delta F_{tr} = 0.1\%$.

Spectroscopic observations of an exoplanet's atmosphere are adversely affected by the spectral lines of its host star, which are orders of magnitude stronger. If the observations are carried out from the Earth's surface, the exoplanet's spectral lines will also be dominated by telluric (or Earth-atmosphere) absorption lines from molecules such as oxygen and water.

However, these issues can be mitigated if the observations are made at very high spectral resolution ($R \sim 100,000$) because this allows the Doppler shift caused by the exoplanet's orbital motion to be resolved, providing a way to separate the planet's spectral lines from those of its host star and the Earth's atmosphere. This is demonstrated in Fig. 1.2, which shows how the spectral lines (at $R = 100,000$) of a toy model of carbon monoxide in the atmosphere of a transiting hot-Jupiter are Doppler shifted by its orbital motion. It also shows telluric lines, which remain at a constant wavelength over time. It does not show stellar lines because there are no stellar lines in this wavelength range, but if there were, they would appear similar to the telluric lines. During transit, at around 0 orbital phase, the planet's spectral lines trace a diagonal line as they are blueshifted, then redshifted. The planet's spectral lines are not visible at the secondary eclipse (phase 0.5) because the planet is behind its host star at that time.

Slit spectrographs, such as those used for this thesis, achieve high spectral resolutions by using narrow entrance slits that reject some star light. Additionally, at high spectral resolutions, the light is more dispersed, which reduces the number of photons landing on a given pixel on the CCD. Therefore, bright sources or long exposure times are needed to reach high signal to noise ratios.

55 Cancri e is one of the few currently known transiting hot super-Earths that orbits a star that is bright enough to be characterised with high-resolution spectroscopy. However, the recently launched Transiting Exoplanet Survey Satellite (TESS) (Ricker et al. 2016) is expected to find several hot super-Earths and disintegrating rocky exoplanets around brighter stars (Barclay et al. 2018).

1.6 Disintegrating rocky exoplanets

Small rocky exoplanets with temperatures on the order of 2,000 K can actively disintegrate and produce 'comet-like' dust tails. Since the dust originates from the

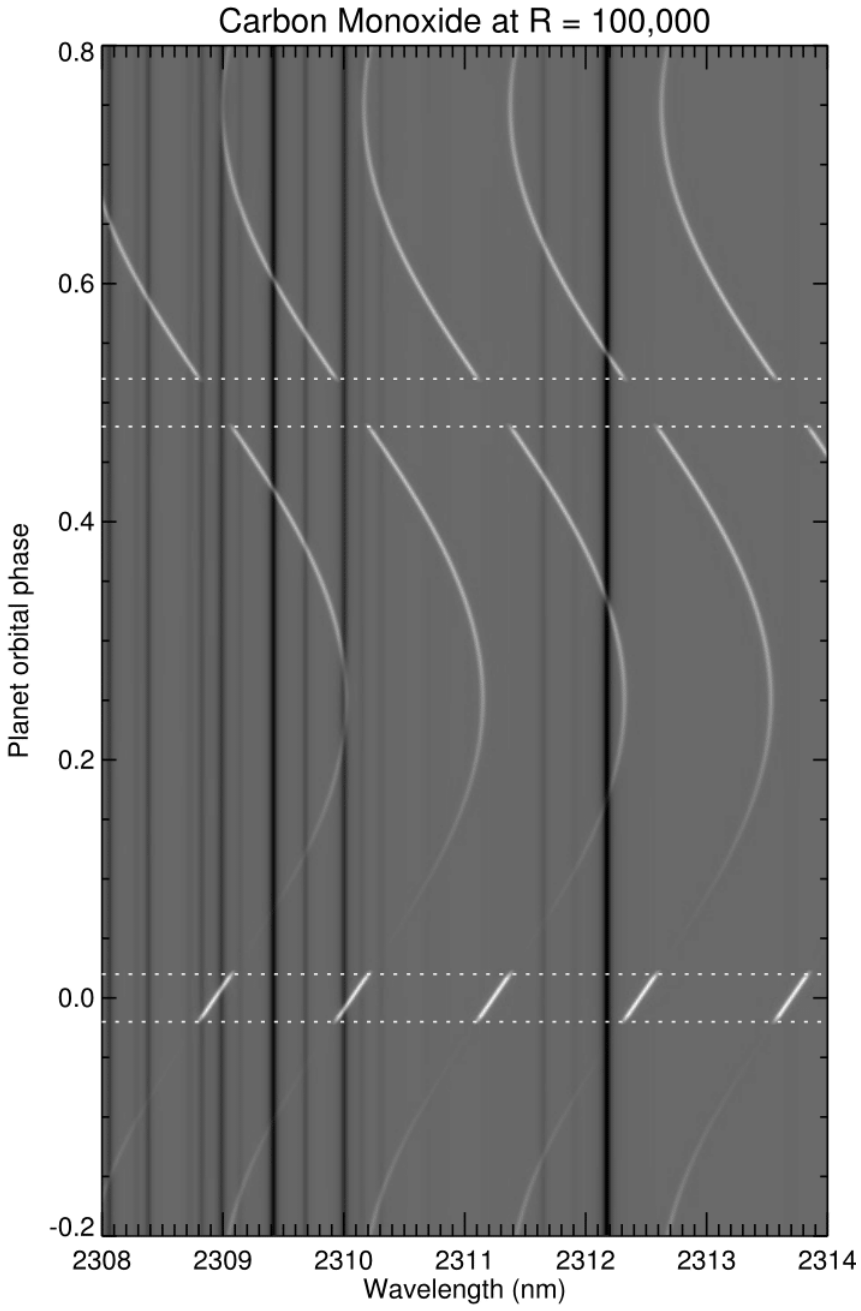

Figure 1.2: A toy model of the spectrum (at $R = 100,000$) of carbon monoxide in the atmosphere of a transiting hot-Jupiter, as a function of orbital phase (vertical axis). Image credit: Matteo Brogi.

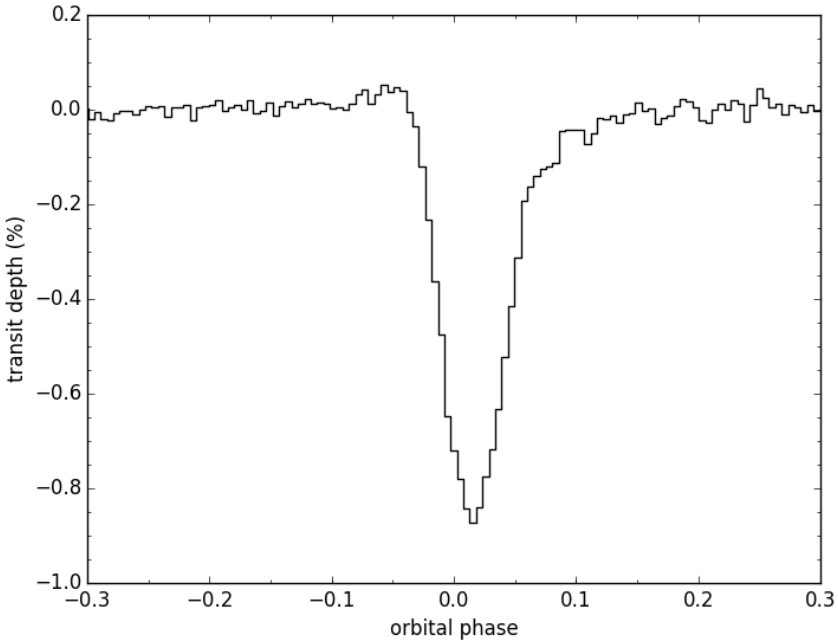

Figure 1.3: The Kepler average long cadence light curve of Kepler-1520 b, produced by the analysis of van Werkhoven et al. (2014).

surface of the planet, these objects offer an unparalleled opportunity to observationally constrain the surface composition of the planet.

To date, three such planets around main-sequence stars and one around a white dwarf have been discovered from Kepler light curves: Kepler-1520 b (also known as KIC 12557548 b) (Rappaport et al. 2012), KOI-2700 b (Rappaport et al. 2014), K2-22 b (Sanchis-Ojeda et al. 2015) and WD 1145+017 (Vanderburg et al. 2015). Their transit light curves are asymmetrical and exhibit dust forward scattering features. They also exhibit transit depths that vary from approximately zero to 1.4%. This variability suggests that the mass-loss rate from the planet also varies over orbital timescales. The average transit light curve of Kepler-1520 b (the first of these planets to be discovered) is shown in Fig. 1.3, where its forward scattering feature at ingress and extended egress are apparent.

1.6.1 Mass-loss mechanism

The leading idea for the mechanism responsible for causing the mass-loss from disintegrating rocky exoplanets is a thermal wind that is launched from the ap-

proximately 2,000 K surface (Perez-Becker & Chiang 2013). As the wind expands and cools, dust grains condense out of a fraction of the gas and are dragged away from the planet by the remaining escaping gas.

This mass-loss could be self-regulating because:

1. An episode of high mass-loss would result in more dust in the planet's atmosphere, which would absorb more stellar flux, reducing the flux received by the surface.
2. The reduced flux will decrease the surface vapour pressure, and hence reduce the outward flow of dust being transported into the upper atmosphere, resulting in a low mass-loss episode.
3. This low mass-loss episode will lead to a clear atmosphere with less dust in the atmosphere to absorb the stellar flux, increasing the vapour pressure and leading back to a period of high mass-loss (Step 1).

This cycle could produce some of the observed variability in transit depth. However, it has also been qualitatively suggested that it may be punctuated with unpredictable outbursts from volcanoes or geysers (Rappaport et al. 2012; Perez-Becker & Chiang 2013), potentially allowing the planet's geophysics to be probed.

Perez-Becker & Chiang (2013) argue that the thermal wind has typical velocities of approximately 1 km s^{-1}. This is comparable to the minimum particle ejection velocity of 1.2 km s^{-1} that was derived in Chapter 3 of this thesis. We search for gas that may have been lost in the thermal wind of K2-22 b (or produced by the sublimation of dust in its tail) in Chapter 5 of this thesis.

1.6.2 Dust particle dynamics

The composition and size of dust particles in the tails of disintegrating hot rocky exoplanets can be observationally constrained (e.g. van Lieshout et al. 2016). Since they originate from the planet, their composition must be related to that of the surface of the planet. However, interpreting how the compositions are connected requires an understanding of the evolution of the dust tails. Their length and morphology are determined by the dynamics of the individual particles in the tail, which is relatively well understood for simple cases.

Their motion is mainly governed by the balance of the stellar radiation pressure force with the stellar gravitational force, which both decrease with the inverse square of the distance from the star (e.g. Rappaport et al. 2012; van Lieshout et al. 2016). This results in the particle effectively experiencing a reduced gravitational field, $g_{\rm eff}$, given by

$$g_{\rm eff} = \frac{GM_s(1-\beta)}{r^2} \tag{1.7}$$

where G is the universal gravitational constant, M_s is the mass of the star, r is the radial distance from the star and β is the ratio of stellar radiation pressure force to stellar gravitational force

$$\beta(s) = \frac{F_{rad}}{F_{grav}} \tag{1.8}$$

where β depends only on the particle size, s, for a given composition. It can be seen that the effective gravity that the particles experience, g_{eff}, is the gravity that the particles would experience if the host star's mass were reduced by a factor of $(1-\beta)$.

In the ideal case where a particle's ejection velocity from the planet is comparable to the planet's escape velocity, it will go into an elliptical Keplerian orbit with periastron at the point where the particle was released (Rappaport et al. 2014).

For such an orbit, the eccentricity can be calculated as

$$e = \frac{\beta}{1-\beta} \tag{1.9}$$

the dust particle's orbital semi-major axis, a_d, relative to that of the planet, a_p, is

$$a_d = a_p \frac{1-\beta}{1-2\beta} \tag{1.10}$$

and the dust particle's orbital angular frequency, ω_d, relative to that of the planet, ω_p, is

$$\omega_d = \omega_p \frac{(1-2\beta)^{\frac{3}{2}}}{1-\beta}. \tag{1.11}$$

These equations indicate that a dust particle will be on a bound orbit if $\beta < 0.5$ because if $\beta = 0.5$, $e = 1$, a_d/a_p goes to infinity and $\omega_d/\omega_p = 0$. With increasing β (while $\beta < 0.5$), the dust particle's eccentricity and orbital semi-major axis increase, while its orbital angular velocity decreases. These all result in the dust particle drifting away from the planet.

However, the stellar radiation causes the dust particles to sublimate, which changes their size, s, and corresponding value of $\beta(s)$. Therefore, these orbital elements evolve over the lifetimes of the dust particles.

For spherical dust grains, the value of β is given by

$$\beta(s) = \frac{3}{16\pi cG} \frac{L_s}{M_s} \frac{\bar{Q}_{pr}(s)}{\rho_d s} \tag{1.12}$$

where c is the speed of light, G is the universal gravitational constant, L_s is the luminosity of the host star, M_s is the mass of the host star, ρ_d is the density of

the dust, s is the dust grain's radius and $\bar{Q}_{pr}(s)$ is the radiation pressure efficiency averaged over the stellar spectrum. $\bar{Q}_{pr}(s)$ depends on the dust's refractive index and can be calculated from Mie theory (Mie 1908; Burns et al. 1979).

While $\beta(s)$ varies depending on the dust composition, the profile of β as a function of s, for all compositions, generally have the same shape. Their peak values for $\beta(s)$ generally occur when the grains have sizes, s_p, that are similar to the host star's peak wavelength (Burns et al. 1979). For the spectrum of Kepler-1520, this results in $\beta(s)$ being largest for particles of radii approximately $0.1 - 0.5$ μm (van Lieshout et al. 2014).

Going to larger grain sizes, Mie theory converges to the limit of geometric optics, where $\bar{Q}_{pr}(s)$ essentially becomes a constant value. This results in $\beta(s)$ linearly decreasing with increasing particle size (i.e. $\beta(s) \propto s^{-1}$). For particle sizes less than s_p, $\beta(s)$ decreases because the particles are too small to significantly absorb or scatter photons at the peak wavelength of the host star's spectrum (Burns et al. 1979). Therefore, for typical initial particle radii of approximately 1 μm, sublimation will cause $\beta(s)$ to increase then decrease.

The orbital dynamics of the dust particles is not as well understood in more complicated situations like when the tail is optically thick, providing significant self-shielding. This is investigated in Chapter 4 of this thesis.

1.7 This thesis

This thesis deals with observational and numerical simulation techniques to gain insight into hot rocky exoplanets and move towards determining observational constraints on the geophysical properties of these enigmatic worlds.

1.7.1 Chapter 2

We analysed high dispersion (R $\sim$ 100,000) spectra of five transits of the hot rocky super-Earth, 55 Cancri e, to search for Na and Ca^+ in its atmosphere or exosphere. One transit was observed with UVES/VLT, two were observed with HARPS/ESO 3.6 m and two were observed with HARPS-N/TNG. We used the fact that the planet's radial velocity changed from -57 to $+57$ km s^{-1} during transit to separate its lines from the stellar spectral lines and used a principal component analysis (PCA) to remove the variable telluric lines. By combining all datasets, we detect a signal potentially associated with sodium in the planet's exosphere to a significance of 3σ. Combining the four HARPS/HARPS-N transits that include the Ca^+ H and K lines, we find a potential signal of Ca^+ to a significance of 4.1 σ. However, this signal originates entirely from a single data set, where it has a significance of 4.9σ. We estimate the p-values associated with these signals to be too high to al-

low us to claim definitive detections so we only report them as potential detections worthy of follow-up observations.

1.7.2 Chapter 3

We simulated the dust tail of the disintegrating rocky exoplanet Kepler-1520 b with a dust particle dynamics code and the radiative transfer code, MCMax3D. We found that the transit depth was wavelength independent for optically thick tails. Therefore, a temporal variation in the optical depth of the tail can potentially explain why only some multi-wavelength observations have detected a wavelength dependence in transit depth. We also derived a minimum particle ejection velocity of 1.2 km s^{-1} and found that we required mass-loss rates of $7 - 80$ $M_{\oplus}$ Gyr^{-1} to produce the observed transit depths. However, these mass-loss rates are higher than those derived with other models and may result in planet lifetimes that are inconsistent with the observed sample of planets.

1.7.3 Chapter 4

We extended the model that was developed for Chapter 3 so that it approximated self-shielding within the tail, to investigate the morphology of optically thick tails. The self-shielding reduced the radiation flux received by shielded particles, which reduced the radiation pressure they experienced and their sublimation rates. To reproduce the average transit depth of Kepler-1520 b with the self-shielding model, we required mass-loss rates of $3 - 3.9$ $M_{\oplus}$ Gyr^{-1}. However, we also found that unless the intrinsic sublimation rate was assumed to be very high, it was easy for shielded particles to survive for more than one orbit, violating the lack of correlation between consecutive transit depths found by van Werkhoven et al. (2014).

1.7.4 Chapter 5

We observed four transits of the disintegrating rocky exoplanet K2-22 b with X-shooter/VLT to obtain intermediate resolution spectra to search for gas that was directly lost from the planet or produced by the sublimation of dust particles in the tail. We focussed on the sodium D lines and the ionized calcium near-infrared triplet as these produce the strongest absorption lines in comets, despite their low abundances. We did not detect the species and by injecting artificial signals we derived 5σ upper-limits with absorption relative to the stellar spectrum from sodium and ionized calcium of 9% and 1.6%, respectively. These limits indicate low gas-loss limits compared to the estimated average dust mass-loss derived for this system. We suggest that the probed gases are probably accelerated by the stellar wind and radiation pressure, leading to very broad and difficult to detect blueshifted sig-

nals with widths of hundreds of km s^{-1}. We searched for such signals in our data but did not detect them.

1.8 Future outlook

The main limitation on studying hot rocky exoplanets is achieving high signal-to-noise ratios (SNRs) in transit light curves and transmission spectroscopy. This is particularly relevant for disintegrating rocky exoplanets because their individual transit light curves are not of a sufficiently high SNR to reveal features such as forward scattering peaks that can be fit with models, so they are averaged to increase SNR (van Werkhoven et al. 2014). However, their transit light curves are known to be highly variable, so the average light curve, and the physical properties derived from it, may not accurately reflect the individual cases.

One way that higher SNRs can be achieved is by using large telescopes such as the upcoming Extremely Large Telescope (ELT) and Thirty Meter Telescope (TMT), which are planned to start operating in 2024[2] and 2027[3], respectively. However, another potential avenue is opened by TESS, which is expected to discover several hot, potentially disintegrating, rocky exoplanets orbiting bright stars (Barclay et al. 2018) that can be characterised in detail with current facilities.

Once we are able to observe high SNR transit light curves of disintegrating rocky exoplanets in several wavelength bands, more accurate dust-tail models that include higher order effects can be quantitatively compared to the observations. These additional higher order effects could potentially include modelling the effect of gas-pressure on the dust-particle dynamics and coupling the dust-tail dynamics models to physically inspired models of mass-loss from the planet, so that the properties of the mass-loss mechanism can be constrained.

For hot rocky super-Earths, high SNR transmission spectra will allow robust detections of chemical species in their atmospheres, that will likely be strongly linked to their rocky surface compositions (e.g. Schaefer & Fegley 2009). Going beyond this, robust detections of several species will make it possible to meaningfully constrain their formation and migration histories by comparing to models that relate a planet's current atmospheric abundances to the conditions in its protoplanetary disk during its formation (e.g. Madhusudhan et al. 2016; Cridland et al. 2016).

[2] `http://iopscience.iop.org/article/10.1088/2058-7058/29/8/21`

[3] `https://www.tmt.org/page/timeline?category=Observatory+Construction`

Bibliography

Barclay, T., Pepper, J., & Quintana, E. V. 2018, ArXiv e-prints, arXiv:1804.05050

Borucki, W. J., Koch, D., Basri, G., et al. 2010, Science, 327, 977

Boss, A. P. 1997, Science, 276, 1836

Burns, J. A., Lamy, P. L., & Soter, S. 1979, Icarus, 40, 1

Chambers, J. E. 2009, Annual Review of Earth and Planetary Sciences, 37, 321

Chatterjee, S., Ford, E. B., Matsumura, S., & Rasio, F. A. 2008, ApJ, 686, 580

Cridland, A. J., Pudritz, R. E., & Alessi, M. 2016, MNRAS, 461, 3274

Dawson, R. I. & Johnson, J. A. 2018, ArXiv e-prints, arXiv:1801.06117

Ehrenreich, D., Bourrier, V., Bonfils, X., et al. 2012, A&A, 547, A18

Esteves, L. J., de Mooij, E. J. W., Jayawardhana, R., Watson, C., & de Kok, R. 2017, AJ, 153, 268

Gillon, M., Demory, B.-O., Benneke, B., et al. 2012, A&A, 539, A28

Gillon, M., Triaud, A. H. M. J., Demory, B.-O., et al. 2017, Nature, 542, 456

Guenther, E. W., Cabrera, J., Erikson, A., et al. 2011, A&A, 525, A24

Howell, S. B., Sobeck, C., Haas, M., et al. 2014, PASP, 126, 398

Ito, Y., Ikoma, M., Kawahara, H., et al. 2015, ApJ, 801, 144

Jackson, B., Adams, E., Heller, R., & Endl, M. 2018, ArXiv e-prints

Kaltenegger, L. 2011, Scale Height, ed. M. Gargaud, R. Amils, J. C. Quintanilla, H. J. J. Cleaves, W. M. Irvine, D. L. Pinti, & M. Viso (Berlin, Heidelberg: Springer Berlin Heidelberg), 1492–1492

Killen, R., Cremonese, G., Lammer, H., et al. 2007, Space Sci. Rev., 132, 433

Koch, D. G., Borucki, W. J., Basri, G., et al. 2010, ApJ, 713, L79

Lin, D. N. C., Bodenheimer, P., & Richardson, D. C. 1996, Nature, 380, 606

Lin, D. N. C., Woosley, S. E., & Bodenheimer, P. H. 1991, Nature, 353, 827

Madhusudhan, N., Agúndez, M., Moses, J. I., & Hu, Y. 2016, Space Science Reviews, 205, 285

Mie, G. 1908, Annalen der Physik, 330, 377

Miguel, Y., Kaltenegger, L., Fegley, B., & Schaefer, L. 2011, ApJ, 742, L19

Mura, A., Wurz, P., Schneider, J., et al. 2011, Icarus, 211, 1

Perez-Becker, D. & Chiang, E. 2013, MNRAS, 433, 2294

Pollack, J. B., Hubickyj, O., Bodenheimer, P., et al. 1996, Icarus, 124, 62

Rappaport, S., Barclay, T., DeVore, J., et al. 2014, ApJ, 784, 40

Rappaport, S., Levine, A., Chiang, E., et al. 2012, ApJ, 752, 1

Ricker, G. R., Vanderspek, R., Winn, J., et al. 2016, in Space Telescopes and Instrumentation 2016: Optical, Infrared, and Millimeter Wave, Vol. 9904, 99042B

Sanchis-Ojeda, R., Rappaport, S., Pallè, E., et al. 2015, ApJ, 812, 112

Schaefer, L. & Fegley, B. 2009, ApJ, 703, L113

Schlichting, H. E. 2014, ApJ, 795, L15

Schlichting, H. E. 2018, ArXiv e-prints

Tsiaras, A., Rocchetto, M., Waldmann, I. P., et al. 2016, ApJ, 820, 99

van Lieshout, R., Min, M., & Dominik, C. 2014, A&A, 572, A76

van Lieshout, R., Min, M., Dominik, C., et al. 2016, A&A, 596, A32

van Werkhoven, T. I. M., Brogi, M., Snellen, I. A. G., & Keller, C. U. 2014, A&A, 561, A3

Vanderburg, A., Johnson, J. A., Rappaport, S., et al. 2015, Nature, 526, 546

Ward, W. R. 1997, Icarus, 126, 261

Wolszczan, A. & Frail, D. A. 1992, Nature, 355, 145

Wright, J. T. 2017, Radial Velocities as an Exoplanet Discovery Method, ed. H. J. Deeg & J. A. Belmonte (Springer Living Reference Work), 4